Hydrol. Earth Syst. Sci. Discuss., 6, 5505–5536, 2009
www.hydrol-earth-syst-sci-discuss.net/6/5505/2009/

Hydrology and Earth System Sciences Discussions

Papers published in *Hydrology and Earth System Sciences Discussions* are under open-access review for the journal *Hydrology and Earth System Sciences*

Assimilation of satellite information in a snowpack model to improve characterization of snow cover for runoff simulation and forecasting

L. S. Kuchment[1], **P. Romanov**[2], **A. N. Gelfan**[1], **and V. N. Demidov**[1]

[1]Water Problem Institute of the Russian Academy of Sciences, Moscow, Russia
[2]University of Maryland, College Park, MD, USA

Received: 22 July 2009 – Accepted: 3 August 2009 – Published: 12 August 2009

Correspondence to: A. N. Gelfan (hydrowpi@aqua.laser.ru)

Published by Copernicus Publications on behalf of the European Geosciences Union.

Abstract

A new technique for constructing spatial fields of snow characteristics for runoff simulation and forecasting is presented. The technique incorporates satellite land surface monitoring data and available ground-based hydrometeorological measurements in a physical based snowpack model. The snowpack model provides simulation of temporal changes of the snow depth, density and water equivalent (SWE), accounting for snow melt, sublimation, refreezing melt water and snow metamorphism processes with a special focus on forest cover effects. The model was first calibrated against available ground-based snow measurements and then was applied to calculate the spatial distribution of snow characteristics using satellite data and interpolated ground-based meteorological data. The remote sensing data used in the model consist of products derived from observations of MODIS and AMSR-E instruments onboard Terra and Aqua satellites. They include daily maps of snow cover, snow water equivalent (SWE), land surface temperature, and weekly maps of surface albedo. Maps of land cover classes and tree cover fraction derived from NOAA AVHRR were used to characterize the vegetation cover. The developed technique was tested over a study area of approximately 200 000 km^2 located in the European part of Russia (56° N to 60° N, and 48° E to 54° E). The study area comprises the Vyatka River basin with the catchment area of 124 000 km^2. The spatial distributions of SWE, obtained with the coupled model, as well as solely from satellite data were used as the inputs in a physically-based model of runoff generation to simulate runoff hydrographs on the Vyatka river for spring seasons of 2003, 2005. The comparison of simulated hydrographs with the observed ones has shown that suggested procedure gives a higher accuracy of snow cover spatial distribution representation and hydrograph simulations than the direct use of satellite SWE data.

HESSD

6, 5505–5536, 2009

1 Introduction

Snow cover formation and snowmelt processes play a significant role in the hydrological cycle and in the heat exchange between the land surface and the atmosphere. Information on the snow spatial characteristics is important for predicting snowmelt floods and for water resources management. However, the existing network of ground-based stations most often does not provide measurements of snow cover properties at the required spatial and temporal resolution.

A promising opportunity to enhance the assessment and monitoring of spatial and temporal variability of snow characteristics particularly in areas with a sparse network of meteorological stations consists in the use of the satellite observations. Reliability of satellite measurements of snow cover characteristics and their spatial resolution have noticeably improved during the last years. To a large extent this improvement was due to the launch of several new satellite observing systems with advanced capabilities such as the Moderate Resolution Imaging Spectroradiometer (MODIS) onboard Terra and Aqua satellites and the Advanced Microwave Sounding Radiometer for Earth Observing System (EOS) satellites (AMSR-E) onboard Aqua (König et al., 2001; Hall et al., 2002). Improvements were also achieved due to the development and implementation of advanced techniques of satellite data interpretation, particularly techniques that combine information from different satellites and different satellite sensors (Romanov et al., 2000; Tait et al., 2000). Still, potentials for accurate satellite measurements of snow characteristics and the frequent updates are limited by a number of environmental factors such as cloudiness, land cover type, snow properties, terrain peculiarities, etc. Clouds create discontinuity in the spatial distribution and in time series of snow data. Large errors in the satellite measurements of snow characteristics are often observed in the mountains. Dense forest vegetation complicates snow cover identification and mapping due to snow interception and ability to mask snow cover on the forest floor.

A possible way to improve characterization of the snow cover spatial distribution and temporal variability consists in coupling satellite data with ground-based hydromete-

HESSD
6, 5505–5536, 2009

orological measurements and hydrological models describing snow pack processes. Several studies focused at the assimilation of satellite-derived snow observations into hydrological models have been carried out during the last decade. Rodell and Houser (2004) proposed an assimilation scheme combining the fractional snow covered area (SCA) observations retrieved from MODIS with a snow cover model. The scheme was used to adjust the simulated SWE in the spatial grid cells using the MODIS-derived values of SCA. Clark et al. (2006) have used the SCA information to update snow accumulation, snowmelt and to characterize variability of sub-grid SWE in the model of snow accumulation and ablation processes. A Bayesian scheme for assimilation of satellite-based SCA into the snow model using prior information on snow depletion was presented by Kolberg et al. (2006). Recently, US National Operational Hydrologic Remote Sensing Center (NOHRSC) has developed a Snow Data Assimilating System (SNODAS) where the ground-based, airborne and satellite snow observations were assimilated into the snow model to obtain the snow cover characteristics at 1 km spatial resolution and hourly temporal resolution (Carroll et al., 2006).

In this paper we present a technique for constructing spatial fields of snow cover characteristics using satellite data products combined with available standard meteorological data and a physical based model of snow pack processes. The model is first calibrated against available snow measurements at meteorological stations. Next, it is applied to simulate the spatial distribution of snow characteristics using satellite data and interpolated ground-based meteorological data as input. The modeled spatial distribution of snow cover is incorporated in a distributed physical based model of runoff generation to calculate snowmelt runoff hydrographs. The correspondence of simulated and observed hydrographs may be considered as an indicator of the accuracy of reconstructed fields of snow characteristics.

The development of the new snow modeling technique and its testing was performed over a study area of about 200 000 km^2 located in the European part of Russia within 56° N to 60° N and 48° E to 54° E. The study area incorporates the Vyatka River basin with the the catchment area of 124 000 km^2) (Fig. 1).

The region has flat terrain and mixed vegetation cover. In its northern part more than 80% of the area is covered by forests. The southern part is mostly agricultural land with less than 10–15% forest cover fraction (see Fig. 2). In the cold season (October to March) the air temperature typically remains below 0°C. The snow seasons lasts for about 5 months with seldom thaws and maximum snow accumulation attained in the end of March. Maximum values of SWE range from 100–120 mm in the south of the region to up to 200–250 mm in the north. Snow melting usually starts in the third decade of March and ends in the beginning of May.

2 Satellite and ground-based information used in the study

Observations from MODIS and AMSR-E instruments onboard Terra and Aqua satellites are used at NASA to routinely generate various environmental products characterizing the land surface and the Earth's atmosphere. In this study we have used several of these products, namely maps of snow cover, snow water equivalent, land surface temperature and albedo.

Daily global maps of snow water equivalent AE_DySno are derived from observations of the Advanced Microwave Scanning Radiometer (AMSR-E) onboard Aqua satellite. In order to derive SWE an empirical formula is used which relates SWE to the difference of the satellite-observed brightness temperature in 18 GHz and 36 GHz spectral bands at vertical polarization and the forest cover fraction. The estimated accuracy of SWE is 25% (Chang, Rango, 2000). This accuracy may substantially decrease in forested areas and during snow melt when the snowpack is saturated with melt water (Engen et al., 2004). AE_DySno maps are generated on an Equal-Area Scalable Earth Grid (EASE-Grid) with a grid cell size of approximately 25 km. To facilitate assimilation of SWE data in the snow pack model, AE_DySno maps over the study area have been converted to a Platte-Carree (or latitude-longitude) projection with 0.2° grid cell size.

Information on the snow cover distribution was obtained from daily swath-based snow cover maps MOD10_L2 and MYD10_L2 derived correspondingly from MODIS

Terra and MODIS Aqua. Every pixel in the map is classified as snow, snow-free land surface or undetermined. The latter class includes pixels that were obstructed by clouds, did not get enough daylight to be properly classified or did not pass any of data quality control tests. Data over the study area extracted from individual tiles of MOD10_L2 and MYD10_L2 maps and were brought to the Platte Carree projection with the grid step of 0.01°.

Earlier estimates of the accuracy of MODIS-based snow cover maps range from 90% to 98% depending on the season and the surface type (Hall and Riggs, 2007). Most studies report a substantial increase of the percent of errors of snow detection in forested areas (e.g Simic et al., 2004). The results of our analysis of MODIS snow maps agree with these conclusions and clearly demonstrate problems in snow detection in forests. Despite a small size of the study area estimates of the fraction of snow covered area over forested portions of the study region exhibit much larger short-term temporal variations than over non-forested areas (see Fig. 3). Drops in the SCA in early 2003 before the onset of the snowmelt should be attributed to misclassification of snow covered pixels as snow-free. Comparison of graphs in Fig. 3a and b shows that snow misses in MODIS Aqua maps occur more frequently than in the MODIS Terra snow product. Therefore in this study we have used snow maps derived only from MODIS Terra.

Two other parameters used in this study include the land surface temperature and albedo derived from MODIS data. MODIS Terra swath-based product MOD11_L2 incorporates twice a day LST maps in the natural satellite projection. The accuracy of land surface temperature estimates is close to 1°C. Maps of albedo MOD43C1 are derived at 5 km resolution from MODIS-Terra reflective channels data accumulated over 16-day periods. For consistency all LST and albedo data were regridded to the Platte-Carree projection at 0.01° spatial resolution.

Besides current MODIS and AMSR-E data, we have also used static datasets representing correspondingly the type of the land surface, the type and density of the forest vegetation cover. All latter data products are based on observations from

AVHRR aboard NOAA's satellite (Hansen et al., 2000). They have been produced at the University of Maryland Department of Geography and were acquired from http://glcf.umiacs.umd.edu/data.

The full list of the satellite products used in the present work is given in Table 1. Figure 4 shows examples of SWE, SCA, surface temperature and albedo maps. As it can be seen from these maps, the satellite data give opportunity to reveal significant spatial heterogeneities in distribution of considered variables.

Meteorological data were collected from 19 ground-based stations within the study area (Fig. 1). The data included 6-h observations of temperature, humidity, precipitation amount, cloud cover and wind speed.

3 Snow pack model, its calibration and validation using ground-based data

The snow pack model used in this study is a system of vertically averaged equations which includes description of temporal changes of the snow depth, content of ice and content of liquid water taking into account of snow melt, sublimation, refreezing melt water, snow metamorphism. Its brief description is given below. (The model is presented in full in Gelfan et al., 2004 and Kuchment and Gelfan, 2004):

$$\frac{dH}{dt} = \rho_w \left[X_s \rho_0^{-1} - (S + E_s)(\rho_i i)^{-1} \right] - V \quad (1)$$

$$\frac{d}{dt}(iH) = \frac{\rho_w}{\rho_i}(X_s - S - E_s) + S_i \quad (2)$$

$$\frac{d}{dt}(wH) = X_l + S - E_l - R - \frac{\rho_i}{\rho_w} S_i \quad (3)$$

$$c_s \frac{d}{dt}(T_s H) = Q_a - Q_g - \rho_w L S + \rho_i L S_i \quad (4)$$

HESSD
6, 5505–5536, 2009

where H is the snow depth; i and w are the volumetric content of ice and liquid water, respectively; T_s is the temperature of snowpack; S is the snow melt rate; S_i is the rate of freezing of liquid water in snow, E_l is the rate of liquid water evaporation from snow; E_s is the rate of snow sublimation, Q_a is the net heat flux at the snow surface; Q_g is the ground heat flux; X_s and X_l are the snowfall and rainfall rate at the snow surface, respectively; V is the snowpack compression rate; R is the snowmelt outflow from snowpack; c_s is the specific heat capacity of snow; ρ_w, ρ_i, and ρ_0 are the densities of water, ice, and fresh-fallen snow, respectively; L is the latent heat of ice fusion.

The melt rate S of snow is found from the energy balance of the snowpack at T_s=0°C as:

$$S = \begin{cases} \left(Q_a - Q_g\right)\left(\rho_w L\right)^{-1} = \left(Q_{sw} + Q_{lw} - Q_{ls} + Q_T + Q_E + Q_P - Q_g\right)\left(\rho_w L\right)^{-1}, Q_a - Q_g > 0 \\ 0, Q_a - Q_g < 0 \end{cases}, \quad (5)$$

where Q_{sw} is the net short wave radiation; Q_{lw} is the downward long wave radiation; Q_{ls} is the upward long wave radiation from snow; Q_T is the sensible heat exchange; Q_E is the latent heat exchange; Q_P is the heat content of liquid precipitation.

Radiation fluxes are calculated differently depending on the vegetation cover properties. Components of Q_a (in W m^{-2}) for an open site are calculated as follows. The net short wave radiation and downward long wave radiation are expressed with the empirical relationships Eqs. (6)–(9) where the observed air temperature, air humidity, wind speed, precipitation, and cloudiness are used as input:

$$Q_{sw} = Q_0\left(1.00 - \alpha_s\right)\left(1.00 - 0.20N - 0.47N_0\right) \quad (6)$$

where Q_0=1000β is the short-wave radiation flux under clear sky conditions for the day and the hour in question; β is the angle of short-wave radiation above the horizontal in radians, calculated as a function of the local latitude, the declination, and the sun's hour angle; α_s is the snow albedo calculated from

$$\alpha_s = \alpha_0 - \rho_s \rho_w^{-1} \quad (7)$$

α_0 is the empirical coefficient; N and N_0 are the total and the lower level cloudiness (ratiometric), respectively;

$$Q_{lw} = \sigma T_a^4 \left(0.61 + 0.05 e_a^{0.5}\right) (1.00 + 0.12N + 0.12N_0) \quad (8)$$

$$Q_{ls} = \varepsilon_s \sigma T_s^4 \quad (9)$$

where σ is the Stefan-Boltzmann constant ($\mathrm{W\,m^{-2}\,K^{-4}}$); e_a is the air vapor pressure (mb), ε_s is the effective emissivity of the snowpack taken equal to 0.99 in this study

The turbulent fluxes of sensible and latent heat are calculated following Jordan et al. (1999):

$$Q_T = \left(\frac{\rho_a c_a}{r_a} + q_T\right)(T_a - T_s) \quad (10)$$

$$Q_E = \left(\frac{0.622 L_s \rho_a}{P_a r_a} + q_E\right)(e_a - e_s) \quad (11)$$

where r_a is the aerodynamic resistance; e_s is the saturation air vapor pressure at the temperature of snow surface; ρ_0 is the air density; c_a is the specific heat capacity of air; P_a is the atmospheric pressure; L_s is the latent heat of sublimation of ice in the absence of liquid water or the latent heat of vaporisation when liquid water is present in snow; q_T and q_a are the wind-less convection coefficients for the sensible and the latent heat fluxes, respectively. The coefficients q_T and q_a enable heat transfer to occur even when wind speed is zero.

The aerodynamic resistance is calculated as follows (see Price and Dunne, 1976):

$$r_a = \frac{\left[\ln\left(\frac{z-H}{z_0}\right)\right]^2}{\kappa^2 U_z} \times \left(1 + 10|\mathrm{Ri}|\right), \quad (12)$$

HESSD
6, 5505–5536, 2009

where U_z is wind speed at the height z; z_0 is the snow surface roughness assigned as 0.005 m; $\kappa$is von Karman's constant; Ri is the Richardson number estimated as:

$$\mathrm{Ri} = \frac{g(T_a - T_s)(z - H)}{U_z^2 [0.5(T_a + T_s)]}, \quad (13)$$

where $g$is the acceleration due to gravity.

The heat flux Q_P caused by the liquid precipitation is expressed as

$$Q_P = \rho_w c_w T_a X_l \quad (14)$$

where c_w is the specific heat capacity of water.

The ground heat flux Q_g is found from Eq. (28) describing the vertical heat transfer in soil.

At the forest floor Eqs. (6) and (8) are modified to take into account the effect of canopy coverage and the type of vegetation on radiation fluxes. Net short wave radiation (Q^*_{sw}) and downward long wave radiation (Q^*_{lw}) fluxes on sub-canopy snow surface are calculated as:

$$Q^*_{sw} = Q_{sw}(1 - C_c + k_{sw} C_c) \quad (15)$$

$$Q^*_{lw} = C_c Q_{lc} + (1 - C_c) Q_{lw} \quad (16)$$

where C_c is the canopy coverage (ratiometric); k_{sw} is the transmissivity through the canopy; Q_{lc} is the long-wave radiation emitted by the canopy (upward and downward), calculated as $\varepsilon_c \sigma T_c^4$, where T_c is the temperature of canopy (°K) and assumed equal to air temperature; ε_c is the emissivity of the canopy taken as 0.96.

Transmissivity (k_{sw}) is calculated with the following formula:

$$k_{sw} = \exp\left(-Q_{\mathrm{ext}} \mathrm{LAI} \sin^{-1}\beta\right) \quad (17)$$

where LAI is the leaf area index; Q_{ext} is the extinction efficiency estimated as, Q_{ext}=1.08β cos β (β is in radians)

When calculating the turbulent heat exchange under forest canopy, it was assumed that air temperature and air humidity in forest are the same in the forest and in the open area next to the forest. The wind speed in forest U_z^* was defined as:

$$U_z^* = k_u U_z \tag{18}$$

where $k_u$is the coefficient of wind shield calculated as

$$k_u = 0.56 \exp(-2.25 C_c), \quad 0.2 < C_c < 0.9 \tag{19}$$

It was assumed that the precipitation type changes from liquid to solid at the air temperature of 0°C. Depending on the snowfall rate and the forest type part of the snowfall may be intercepted by the forest canopy. For a single snowfall onto a snow-free canopy, the amount of snow intercepted by the forest canopy is defined as:

$$I = I_{\max} \left(1 - \exp \frac{-X_s^*}{I_{\max}}\right) \tag{20}$$

where X_s^* is the snowfall rate above the canopy; $I_{\max}$=S_pLAI$\left(0.27+46\rho_0^{-1}\right)$ is the interception capacity, found as a function of the species snow loading coefficient, S_p. The density of fresh-fallen snow ρ_0 (in kg m^{-3}) depends on the air temperature.

The rate of sublimation of intercepted snow E^i is found from the energy balance of the intercepted snow.

$$E^i = -\left(R_{\text{net}}^i + Q_T^i + Q_P\right)(\rho_w L)^{-1} \tag{21}$$

where R_{net}^i is the net radiation absorbed by the intercepted snow; Q_T^i is the sensible heat exchange for the intercepted snow.

The net radiation, R_{net}^i, absorbed by the intercepted snow is expressed as

$$R_{\text{net}}^i = Q_{sw}\left[1 - \alpha_c - k_{sw}\left(1 - \alpha_s\right)\right] + Q_{lw} + Q_{ls} - 2Q_{lc} \tag{22}$$

where $\alpha_c$is the canopy albedo, $Q_{lc}=\varepsilon_c\sigma T_c^4$, is the long-wave radiation emitted by the canopy (upward and downward), T_c is the temperature of canopy (°K), ε_c is the emissivity of the canopy. In this study α_c and $\varepsilon_c$are taken equal to 0.12 and 0.96 respectively and T_c is assumed equal to the air temperature.

The component Q_T^i is calculated from the ice bulb temperature and wind speed using the approach described in Gelfan et al. (2004).

The rate of liquid water freezing in snowpackS_i is calculated as:

$$S_i = \begin{cases} H\frac{dw}{dt}, T_s{=}0^\circ C \wedge Q_a - Q_g < 0 \wedge \frac{|Q_a-Q_g|}{\rho_i L} \geq H\frac{dw}{dt} \\ \frac{|Q_a-Q_g|}{\rho_i L}, T_s{=}0^\circ C \wedge Q_a - Q_g < 0 \wedge \frac{|Q_a-Q_g|}{\rho_i L} < H\frac{dw}{dt} \\ 0, T_s = 0^\circ C \wedge Q_a - Q_g \geq 0 \\ X_l, T_s < 0^\circ C \end{cases} \quad (23)$$

The snowpack compression rate V is found from (in cm s^{-1}):

$$V = \frac{v_1\rho_s}{\exp(v_2T_s + v_3\rho_s)}\frac{H^2}{2} \quad (24)$$

where ρ_s is the density of snowpack (in g cm^{-3}) equal $\rho_s{=}\rho_i i{+}\rho_w w$; v_1, v_2, and v_3 are the coefficients equal $2.8{\times}10^{-6}$ cm^2 s^{-1} g^{-1}; -0.08°C^{-1}; 21 cm^3 g^{-1}, respectively.

The outflow of liquid water from snow is calculated as:

$$R = \begin{cases} X_l + S - E_l - w_{\max}\frac{dH}{dt}, w = w_{\max} \\ 0, w < w_{\max} \end{cases} \quad (25)$$

where $w_{\max}$ is the holding capacity of snowpack related to its density ρ_s as

$$w_{\max} = 0.11 - 0.11\frac{\rho_s}{\rho_w} \quad (26)$$

The snow pack model was calibrated and validated using available measurements of snow depth at 19 meteorological stations shown in Fig. 1. To calibrate the model we

have used snow depth data obtained during the time period from 1 November 2001 to 30 May 2002. The values of α_0 (Eq. 7), q_T (Eq. 10) and q_a (Eq. 11) were calibrated against snow depth and found equal to 1.01, 0.98 $J\,m^{-2}\,s^{-1}$ and 0.11 $J\,Pa^{-1}\,s^{-1}$, respectively. The calibration was based on the random fitting procedure with prior estimations of parameter ranges which were taken from hydrometeorological literature. The snow depth measurements at the same meteorological stations for the same seasons of 2002–2005 were used to assess the model performance. Figure 5 compares the results of snow depth simulations at several meteorological stations for the cold season of 2002–2003. The standard error of calculated snow depth at all 19 meteorological stations was equal to 7 cm for the training dataset and increased to 9 cm for the independent dataset.

4 Modeling spatial fields of snow characteristics

The calibrated and validated snow pack model was applied to simulate the spatial distribution of snow pack characteristics over the study area during spring seasons of 2003–2005. The model was run for each 0.01° grid cell within the study area for the time period from 1 March to 30 June of every year. To obtain the input data for the snow pack model, the daily ground-based meteorological observation data were interpolated to each pixel with the inverse distance squared method.

In all grid cells where satellite data were available the MODIS-based surface temperature and albedo data were used. In the grid cells where these data were not available, we determined surface temperature and albedo using the relationships Eqs. (4) and (7), respectively.

The initial spatial distribution of SWE for the open or forest-free area was assigned using AE_DySno SWE maps on March 1. The SWE values for forested pixels were estimated by interpolating using the SWE data from open pixels. The interpolated SWE was further multiplied by the factor k_{snow}, representing the average ratio of the pre-melt SWE in the forest to the pre-melt SWE in the neighboring open area. The

value of k_{snow} was obtained from numerical simulation of snow accumulation in the forest with the snow cover model driven by meteorological observations during winter seasons of 2000–2004. The simulation results have shown that in the deciduous forest the value of k_{snow} is close to unity. In coniferous forest this value changes with the canopy coverage. In the sparse coniferous forest, the pre-melt SWE exceeds the SWE in the open area by 9–11% because of smaller snow evaporation and snowmelt during a period of snow accumulation. In the same time, in the dense coniferous forest, interception and sublimation of intercepted snow during this period is larger and thus the pre-melt SWE is 6–13% less than in the open area. The numerical simulations have shown that the variations of the value of k_{snow} from year to year for the same forest area are small and can be negligible.

Assuming that the spatial variability of snow density is much less than variability of SWE, the initial snow density on March 1 was accepted as constant for the whole area and defined from the measurements at the Kirov meteorological station (Fig. 1). The initial volumetric moisture content of snow was assumed equal to zero.

Using the assumptions formulated above, we have simulated daily maps of SWE and snow depth for spring seasons of 2002–2005. Figure 6 presents the maps of simulated distributions of SWE for three dates in the second half of April 2003 corresponding to the period of intensive snowmelt. These maps apparently present the spatial picture of snowmelt dynamics.

The values of SCA determined from simulated SWE maps were compared to the corresponding SCA values derived from NASA MOD10_L2 maps for the snowmelt season of the years 2003 to 2005. Figure 7 shows the temporal change of SCA for two 2500-km^2 regions which are located correspondingly in the south-eastern and north-eastern corners of the study area and have the coniferous forest percentage of 9% and 76% respectively. As it can be seen from this Fig. 7, for the sparsely forested area the calculated values of SCA are close to the values defined from the satellite data while for the area with dense forest there is a significant difference between these values.

To assess the difference between SWE data in NASA AE_DySno maps and the SWE

fields constructed with the developed technique, both SWE fields have been used as the inputs into the physical based model of the Vyatka river runoff generation. The model of runoff generation and the results of its application to calculate hydrographs of spring runoff are discussed in the next section.

5 Using spatial snow characteristics into the distributed model of runoff generation of the Vyatka River basin

The constructed fields of SWE and the AE_DySno SWE maps have been used as the inputs to the physically based model of runoff generation to simulate runoff generation in the Vyatka River basin and to compare the calculated runoff to the observed one.

In this study we have used the model of runoff generation developed in the Water Problems Institute of RAS (Kuchment et al., 1986). The model is based on a finite-element schematization of the catchment area and includes the processes of snow cover formation and snowmelt, freezing and thawing of soil, vertical moisture transfer and evaporation, surface water detention, overland, subsurface and channel flow. In the Vyatka River basin 477 area and 84 channel finite elements have been defined based on the topography of the area, soil and vegetation type distribution as well as the river channel structure and the stream gage allocation (Fig. 8).

To calculate the characteristics of snow cover, the Eq. (1)–(26) were applied. vertical water and heat transfer in the soil associated with soil freezing, thawing and infiltration of water is described with the following equations (Gelfan, 2006)

$$\frac{\partial W}{\partial t} = \frac{\partial}{\partial z}\left(D\frac{\partial \theta}{\partial z} + D_I\frac{\partial I}{\partial z} - K\right) \tag{27}$$

$$c_T\frac{\partial T}{\partial t} = \frac{\partial}{\partial z}\left(\lambda\frac{\partial T}{\partial z}\right) + \rho_w c_w\left(D\frac{\partial \theta}{\partial z} + D_I\frac{\partial I}{\partial z} - K\right)\frac{\partial T}{\partial z} + \rho_w L\frac{\partial W}{\partial t} \tag{28}$$

where W, θ and I are the total water content, liquid water content and ice content of soil, respectively ($W=\theta+\frac{\rho_i}{\rho_w}I$); $K=K(\theta, I)$ is the hydraulic conductivity of the frozen

soil; T is the soil temperature; λ is the thermal conductivity of soil; $D=K\left(\frac{\partial\psi}{\partial\theta}\right)_I$ and $D_I=K\left(\frac{\partial\psi}{\partial I}\right)_\theta$; $\psi=\psi(\theta, I)$ is the capillary potential of the frozen soil; $c_T=c_{\text{eff}}+\rho_w L\frac{\partial\theta}{\partial T}$; c_{eff} is the effective heat capacity of soil $c_{\text{eff}}=\rho_g c_g(1-P)+\rho_w c_w\theta+\rho_i c_i I$; ρ and c are the density and the specific heat capacity, respectively (indexes w, i and g refer to water, ice and soil matrix, respectively); P is the soil porosity.

The capillary potential $\psi=\psi(\theta, I)$ and the hydraulic conductivity $K=K(\theta, I)$ of the frozen soil are determined from the relations proposed in Gelfan (2006). Equations (27)–(28) are numerically integrated by an implicit, four-point finite difference scheme. The corresponding difference equations were solved by the double-sweep method.

At the lower boundary of the podzol soils typical for the Vyatka watershed, the impermeable layer is located at the depth of 1.0–2.0 m. The vertical water flux is assumed equal to zero at this boundary. It is also assumed that the horizontal movement of water along the impermeable layer occurs if the soil moisture content exceeds the field capacity, θ_f, of soil. As a result, the horizontal flux, R_g, is calculated as

$$R_g = \frac{\partial}{\partial t}\left[(\theta-\theta_f)\, z_P\right] \tag{29}$$

where z_P is the soil layer in which $\theta>\theta_f$.

The detention of melt water by the depressions at the catchment surface is calculated by the formula assuming exponential distribution of the storage capacity (Kuchment et al., 1986).

The rate of evaporation from an unfrozen, snow-free soil is calculated by the formula presented in Kuchment et al. (2000).

The kinematic wave equations are applied to describe the overland and channel flow. To account for the subsurface flow, the following equations are used (Kuchment et al.,

HESSD
6, 5505–5536, 2009

2000)

$$(P - \theta_f)\frac{\partial h}{\partial t} + \frac{\partial q}{\partial x} = R_g$$
$$q = K_g i_0 h \quad (30)$$

where h is the subsurface flow depth; q is the subsurface flow discharge; $i_0$is the slope of the layer with subsurface flow; K_g is the horizontal hydraulic conductivity. The kinematic wave equations are numerically integrated by the finite-element coupled with the Galerkin method.

To calculate the water movement through the river channel elements, the advection-diffusion equation is applied. This equation is numerically integrated by the four-point implicit difference scheme.

To take into account the subgrid effects, it was supposed that the snow water equivalent and the saturated hydraulic conductivity was gamma-distributed inside the finite element areas. Coefficient of the spatial variation of the saturated hydraulic conductivity was determined from the empirical formula (Kuchment et al., 1986) whereas the subgrid variation of the snow water equivalent was estimated from the fractal relationships (Kuchment and Gelfan, 2001).

Most of the model parameters have been determined using the available measurements of the basin constants including the relief and river channel characteristics, soil and snow constants, vegetation measurements, and from empirical relationships that were derived and tested using mainly Russian experimental data and field observations (Kuchment et al., 1990). Six parameters associated with the processes of infiltration, soil moisture evaporation, detention in basin storage and flood routing have been calibrated against 17 snowmelt flood hydrographs for the period from 1940 till 1959. Two parameters associated with snowmelt have calibrated against snow measurements. Validation was carried out by comparison of the observed and simulated hydrographs of 20 snowmelt flood hydrographs which had not been used for calibration (for the period from 1960 till 1980). The simulated and the observed hydrographs at Vyatskie Polyany city (the outlet gage of the Vyatka basin) for the last ten years of validation

period are presented in Fig. 9. The standard deviation of the observed flood volumes and peak discharges from the simulated ones are equal to correspondingly 1.1 km^3 and 486 $m^3 s^{-1}$. The Nash and Sutcliffe efficiency criterion for the flood volume and discharge simulations are 0.94 and 0.84, respectively.

Two sets of runoff hydrographs of the Vyatka River were calculated using the calibrated and validated model of runoff generation for the floods of 2003 and 2005. The first set of hydrographs was calculated using the constructed fields of SWE as the inputs. The second one used the AE_DySno SWE data as the inputs. In Fig. 10, the calculated hydrograph sets are compared with each other and with the observed hydrographs for three gauges of the Vyatka river: Kirov, Kotelnich, Vyatskie Polyany (see Fig. 1). As it can be seen from Fig. 10, the constructed fields of SWE have provided the satisfactory accuracy of hydrographs simulation. The flood volume and the peak discharge maximum error at Vyatskie Polyany are equal correspondingly to 19% and to 18%. At the same time, utilizing the AE_DySno SWE data leads to significant runoff underestimation. This underestimation can be explained mainly by errors in estimating SWE in forested areas. These results can be viewed as in indication that reconstruction of fields of snow cover properties with the proposed model-based technique improves the representation of spatial distributions of snow characteristics as compared snow cover fields obtained directly from satellite data. The accuracy of the proposed technique to reconstruct snow cover properties can be improved through more comprehensive calibration of the snow pack model against the observed runoff hydrograph.

6 Conclusions

The new approach for constructing spatial fields of snow characteristics has been developed in this study. Within this technique satellite land surface monitoring data and available standard ground-based hydrometeorological measurements are assimilated in the physical based model of snow pack formation. As compared to snow products

derived solely from satellite data the advantage of the new approach to snow characterization consists in a detailed physical description of snow processes which includes the forest cover effects. This allows for obtaining additional information on snow cover that is absent in satellite measurements. The model provides assimilation of available satellite data including small-scale spatial changes of water snow equivalent, fractional snow-covered area, albedo and snow surface temperature, types of the surface land and takes into account the heterogeneities of the river basin and spatial variations of its characteristics. To obtain the input information for the snow pack model, the meteorological data were interpolated from available ground-based observation points to each pixel by the inverse distance squared method. It is reasonable to improve this procedure using the kriging procedures. However, these procedures can have an advantage in our task if there are possibilities to characterize stochastic features of meteorological fields. It is possible to assume that the suggested approach for constructing spatial fields of snow characteristics can help in more fully using of capabilities of distributed physically based models to simulate the spatial peculiarities of river runoff genesis.

Acknowledgement. This research is supported by NASA Grant NNG06GH45G.

References

Carroll, T., Cline, D., Olheiser, C., Rost, A., Nilsson, A., Fall, G., Bovitz, C., and Li, L.: NOAA national snow analysis. Proceedings of the 74th Annual Western Snow Conference, National Operational Hydrologic Remote Sensing Center, National Weather Service, NOAA, Chanhassen, Minnesota, 2006.

Clark, M. P., Slater, A. G., Barrett, A. P., Hay, L. E., McCabe, G. J., Rajagopalan, B., and Leavesley, G. H.: Assimilation of snow covered area information into hydrologic and land-surface models, Adv. Water Resour., 29(11) 1209–1221, 2006.

Chang, A. T. C. and Rango, A.: Algorithm Theoretical Basis Document for the AMSR-E Snow Water Equivalent Algorithm, Version 3.1, Greenbelt, MD, USA, NASA Goddard Space Flight Center, 2000.

Engen, G., Guneriussen, T., and Overrein, Ø.: Delta-K interferometric SAR technique for snow water equivalent (SWE) retrieval, IEEE Geoscience and remote sensing letters, 1(2), 57–61, 2004.
Gelfan, A. N., Pomeroy, J. W., and Kuchment, L. S.: Modelling Forest Cover Influences on Snow Accumulation, Sublimation, and Melt, J. Hydrometeorol., 5(5), 785–803, 2004.
Gelfan, A. N.: Physically based model of heat and water transfer in frozen soil and its parametrization by basic soil data, in: Predictions in Ungauged Basins: Promises and Progress, IAHS Publ., 303, 293–304, 2006.
Hall, D. K., Riggs, G., Salomonson, V., DiGirolamo, N. E., and Bayr, K. J.: MODIS snow cover products, Remote Sens. Environ., 83, 181–194, 2002.
Hall, D. K. and Riggs, G.: Accuracy assessment of the MODIS snow products, Hydrol. Process., 21, 1534–1547, 2007
Hansen, M., DeFries, R., Townshend, J. R. G., and Sohlberg, R.: Global land cover classification at 1-km resolution using a decision tree classifier, Int. J. Remote Sens., 21, 1331–1365, 2000.
Jordan, R. E., Andreas, E. L., and Makshtas, A. P.: Heat budget of snow-covered sea ice at North Pole 4, J. Geophys. Res., 104(C4), 7785–7806, 1999.
Kolberg, S., Rue, H., and Gottschalk, L.: A Bayesian spatial assimilation scheme for snow coverage observations in a gridded snow model, Hydrol. Earth Syst. Sci., 10, 369–381, 2006,
http://www.hydrol-earth-syst-sci.net/10/369/2006/.
König, M., Winther, J. G., and Isacsson, E.: Measuring snow and glacier ice properties from satellite, Rev. Geophys., 39, 1–27, 2001.
Kuchment, L. S., Demidov, V. N., Motovilov, and Yu, G.: A physically based model of the formation of snowmelt and rainfall runoff, IAHS Publ., 155, 27–36, 1986.
Kuchment, L. S., Motovilov, Yu, G., and Nazarov, N. A.: Sensitivity of the hydrological systems, Moscow, Nauka, 1990, (in Russian).
Kuchment, L. S., Gelfan, A. N., and Demidov, V. N.: A distributed model of runoff generation in the permafrost regions, J. Hydrol., 240, 1–22, 2000.
Kuchment, L. S. and Gelfan, A. N.: Statistical self-similarity of spatial variations of snow cover: verification of the hypothesis and application in the snowmelt runoff generation models, Hydrol. Process., 15(21), 3343–3355, 2001.
Kuchment, L. S. and Gelfan, A. N.: Physically based model of snow accumulation and melt in

a forest, Meteorol. Hydrol., 5, 85–95, 2004, (in Russian).
Price, A. G. and Dunne, T.: Energy balance computations of snowmelt in a subarctic area, Water Resour., Res., 12(7), 686–694, 1976.
Rodell, M. and Houser, P. R.: Updating a land surface model with MODIS-derived snow cover, J. Hydrometeorol., 5, 1064–1075, 2004.
Romanov, P., Gutman, G., and Csiszar, I.: Automated monitoring of snow cover over North America with multispectral satellite data, J. Appl. Meteorol., 39, 1866–1880, 2000.
Simic, A., Fernandes, R., Brown, R., Romanov, P., and Park, W.: Validation of VEGETATION, MODIS, and GOES + SSM/I snow-cover products over Canada based on surface snow depth observations, Hydrol. Process., 18, 1089–1104, 2004.
Tait, A. B., Hall, D. K., Foster, J. L., and Armstrong, R. L.: Utilizing multiple datasets for snow-cover mapping, Remote Sens. Environ., 72, 111–126, 2000.

Table 1. List of satellite data products used in the study.

Land surface characteristic	Satellite	Name of Product	Latitude-Longitude Resolution	Time Resolution	Time Period
Snow Water Equivalent	AQUA	NASA_AE_DySno	0.20°×0.20°	Once per day	1 Mar to 30 May 2003 to 2005
Snow Cover	TERRA	NASA_MOD10_L2	0.01°×0.01°	Once per day	1 Mar to 30 May 2002 to 2005
Land Surface Temperature	TERRA	NASA_MOD11_L2	0.01°×0.01°	Twice per day	1 Mar to 30 May 2002 to 2005
Land Surface Albedo	TERRA	NASA_MOD043C1	0.05°×0.05°	16-day product	1 Mar to 30 May 2002 to 2005
Land Cover Classification	NOAA	Land Cover Type	0.01°×0.01°		
Fraction of Evergreen Tree Cover	NOAA	Evergreen Tree Cover	0.01°×0.01°	Static data generated from NOAA AVHRR data	
Tree Cover Fraction	NOAA	Tree Cover Fraction	0.01°×0.01°		

HESSD
6, 5505–5536, 2009

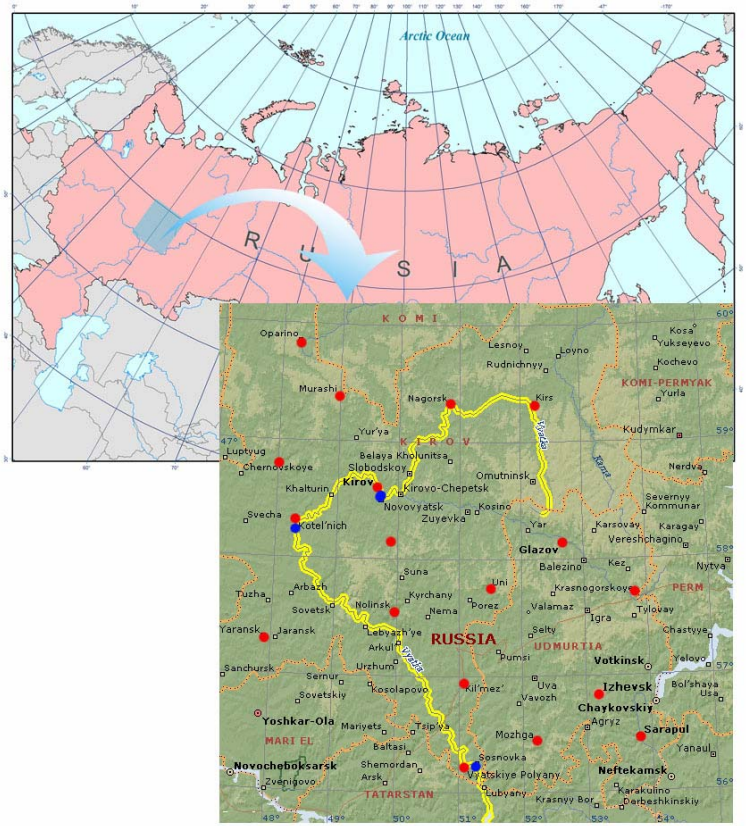

Fig. 1. Location of the study region (red points – meteorological gauges; blue points – hydrological gauges). Vyatka river is highlighted in yellow.

HESSD
6, 5505–5536, 2009

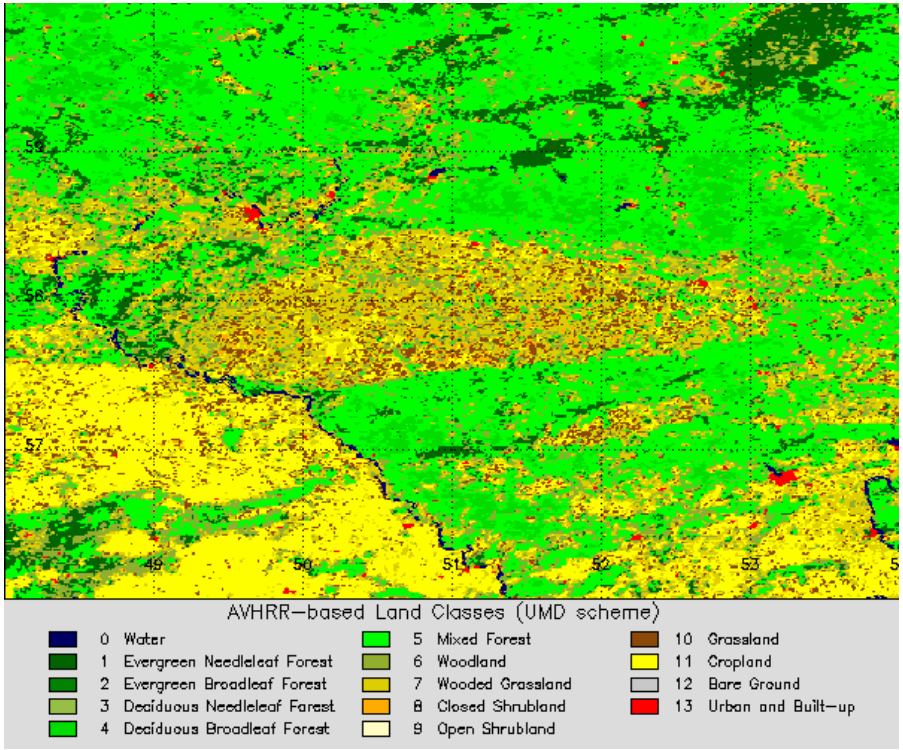

Fig. 2. Land cover classification within the study region.

HESSD
6, 5505–5536, 2009

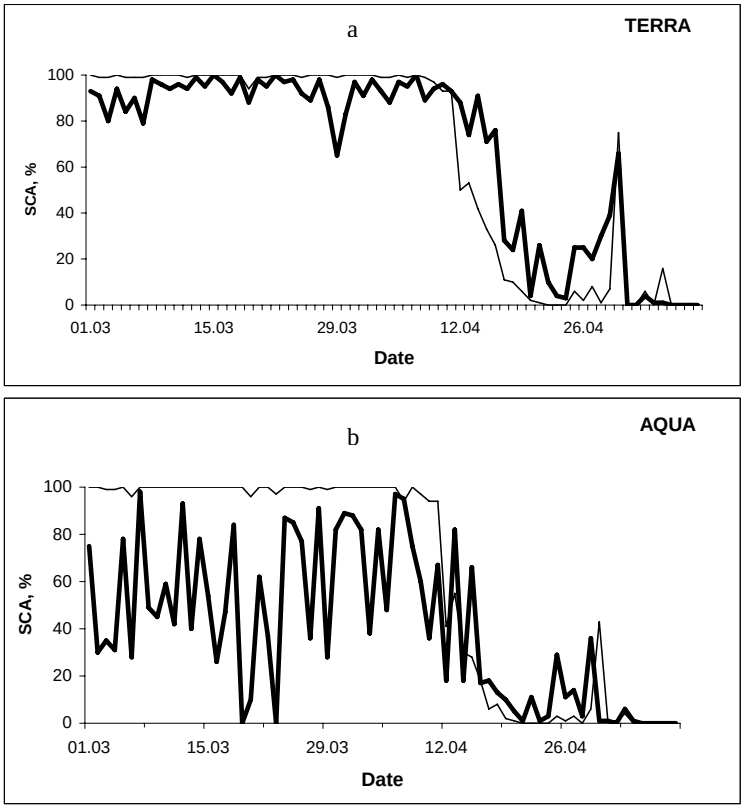

Fig. 3. The fraction of the area covered with snow for open (thin line) and forested (thick line) areas as determined from MODIS AQUA and TERRA snow maps for the melt season of 2003 year.

HESSD
6, 5505–5536, 2009

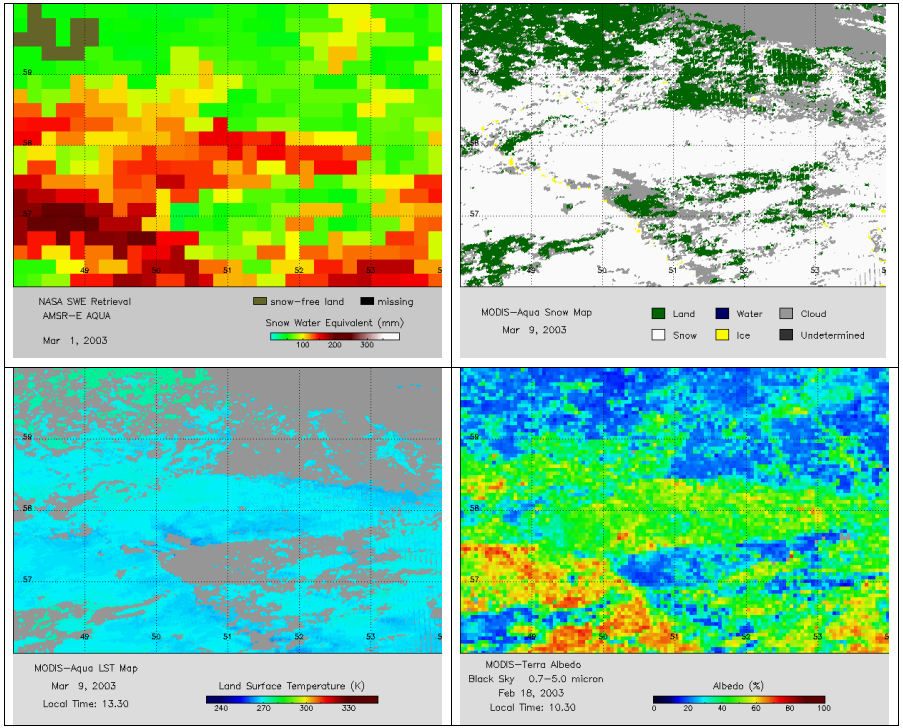

Fig. 4. The satellite-derived maps of SWE, SCA, land surface temperature and albedo for the study area.

HESSD
6, 5505–5536, 2009

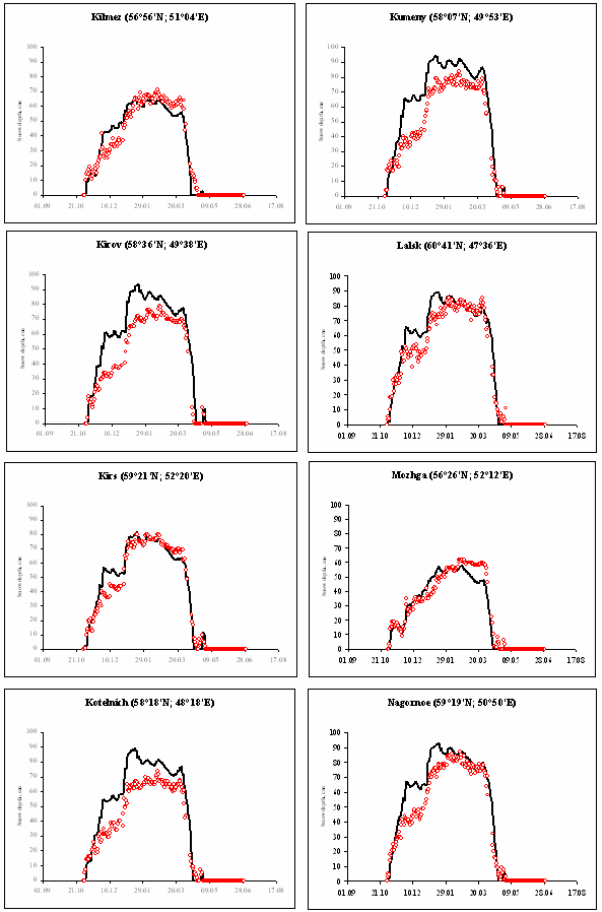

Fig. 5. Seasonal change of the observed (points) and simulated (line) snow depths (in cm) at selected stations within the study area for the season from November 2002 to June 2003.

HESSD
6, 5505–5536, 2009

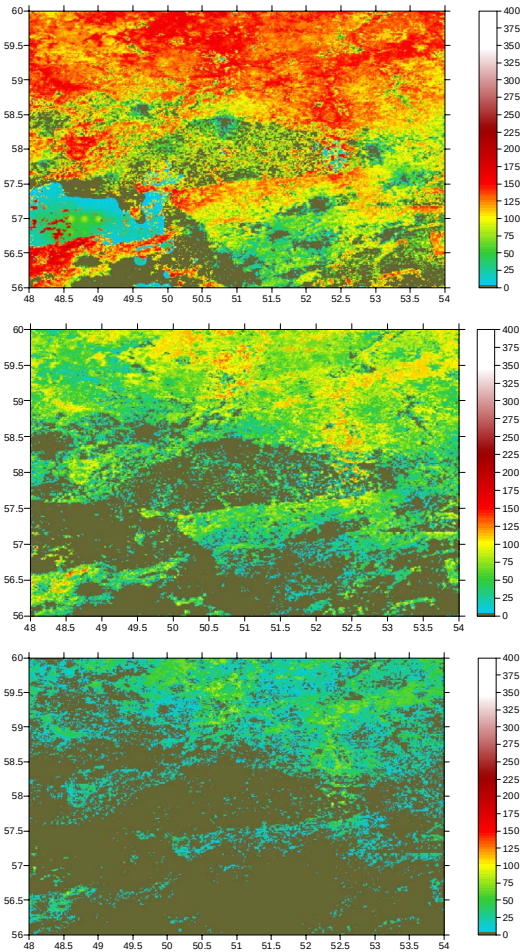

Fig. 6. The calculated maps of SWE (mm) (From the top to the bottom: 14, 19, 22 April 2003).

HESSD

6, 5505–5536, 2009

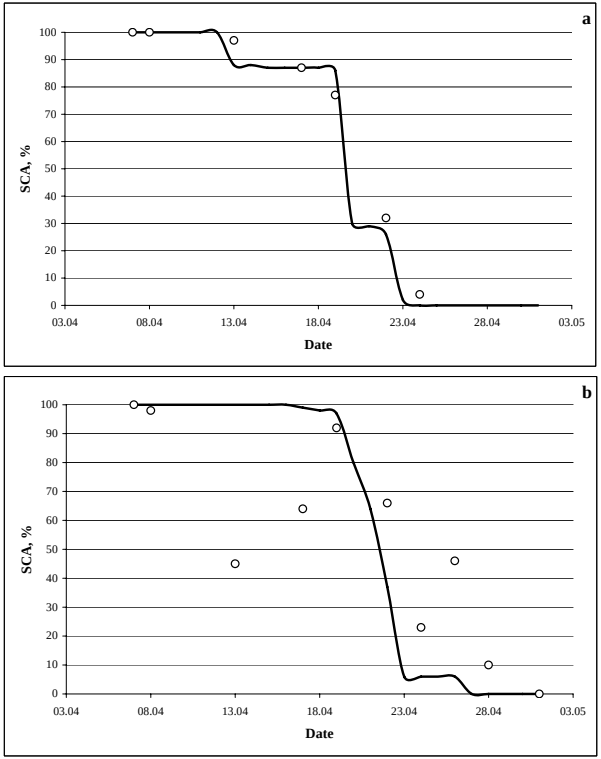

Fig. 7. Changes of the calculated (line) and MODIS-based (points) SCA for two 2500 km^2-areas with different cover percentages of coniferous forest (**a** – 9%; **b** – 76%).

HESSD
6, 5505–5536, 2009

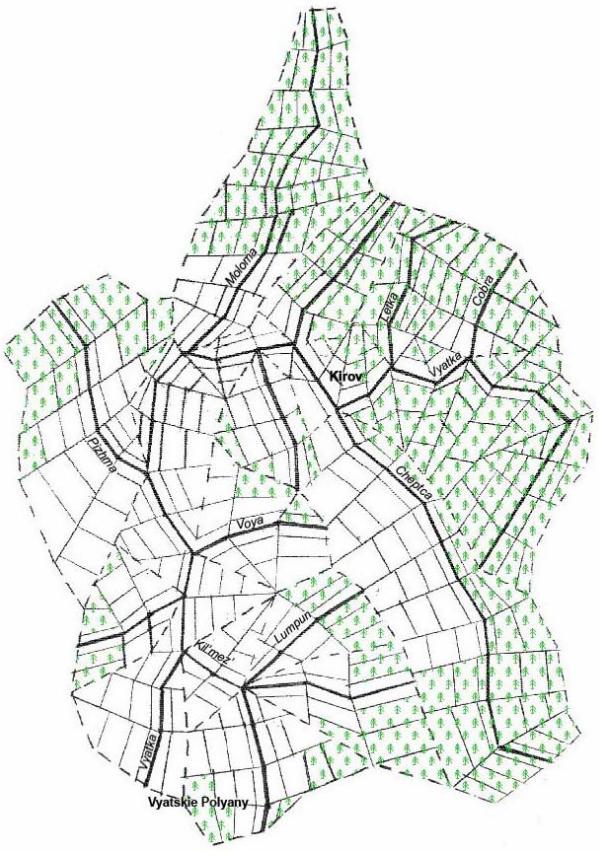

Fig. 8. Finite-element schematization of the Vyatka River basin.

HESSD
6, 5505–5536, 2009

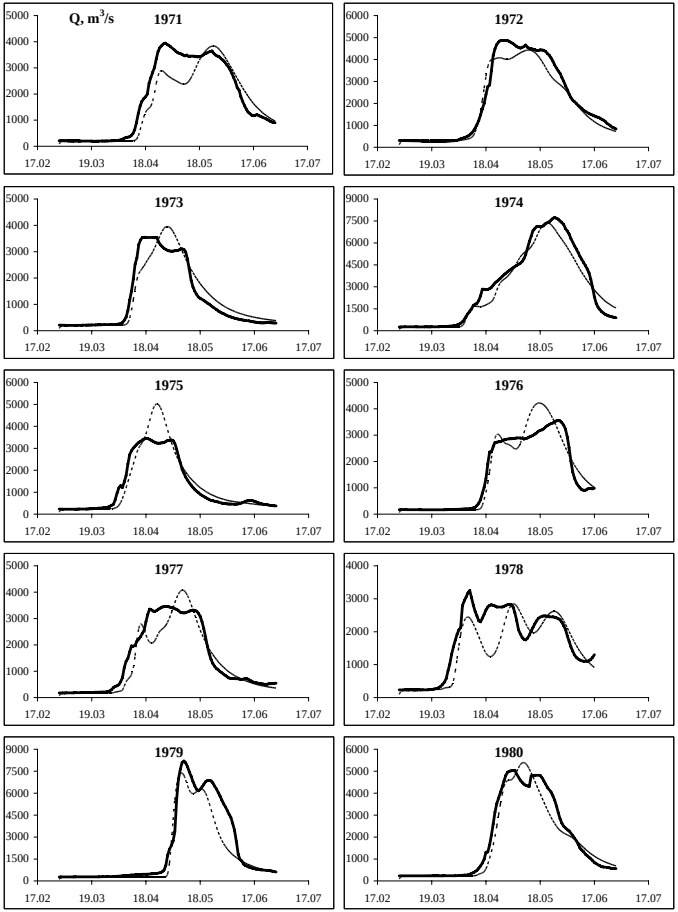

Fig. 9. Comparison of the observed (solid line) and calculated (dashed line) hydrographs at the gauge Vyatskie Polyany of the Vyatka River (the last ten years of validation period).

HESSD
6, 5505–5536, 2009

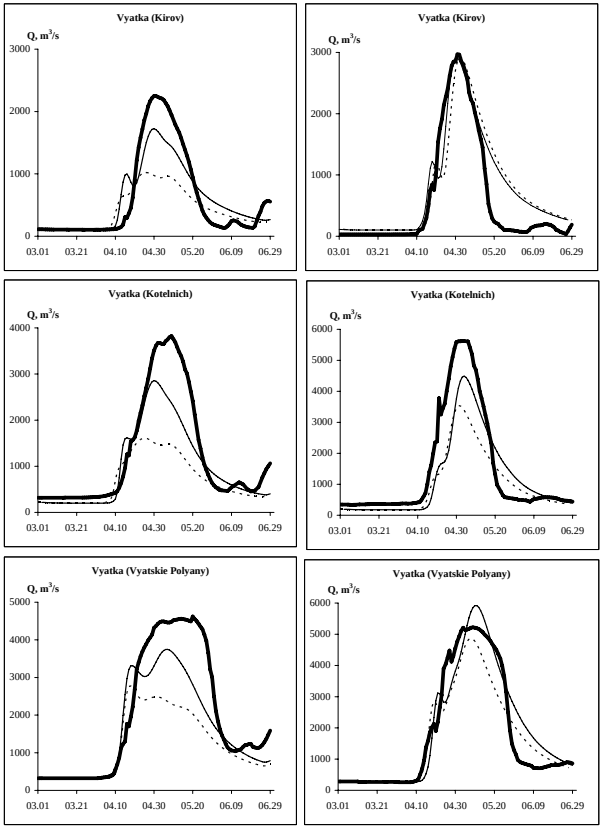

Fig. 10. Comparison of the observed hydrographs (bold line) with the hydrographs calculated from the constructed SWE fields (thin line) and from AE_DySno SWE maps (dashed line) (the left column presents hydrographs of the 2003 flood, the right column presents hydrographs of the 2005 flood).

HESSD
6, 5505–5536, 2009